JOURNAL OF GEOPHYSICAL RESEARCH, VOL. 96, NO. C10, PAGES 18,417–18,423, OCTOBER 15, 1991

Probable Errors in Width Distributions of Sea Ice Leads Measured Along a Transect

J. KEY

Cooperative Institute for Research in Environmental Sciences, University of Colorado, Boulder

S. PECKHAM

Cooperative Institute for Research in Environmental Sciences, and Department of Geology, University of Colorado, Boulder

The degree of error expected in the measurement of widths of sea ice leads along a single transect are examined in a probabilistic sense under assumed orientation and width distributions, where both isotropic and anisotropic lead orientations are examined. Methods are developed for estimating the distribution of "actual" widths (measured perpendicular to the local lead orientation) knowing the "apparent" width distribution (measured along the transect), and vice versa. The distribution of errors, defined as the difference between the actual and apparent lead width, can be estimated from the two width distributions, and all moments of this distribution can be determined. The problem is illustrated with Landsat imagery and the procedure is applied to a submarine sonar transect. Results are determined for a range of geometries, and indicate the importance of orientation information if data sampled along a transect are to be used for the description of lead geometries. While the application here is to sea ice leads, the methodology can be applied to measurements of any linear feature.

1. INTRODUCTION

Polar sea ice is an important factor in the complex interaction of ocean and atmosphere. Reduction in the extent and thickness of sea ice due to global warming, and the consequent increase in the number of cracks in the ice (hereafter "leads"), is expected to further increase global temperatures. This positive feedback is a result of reduced albedo and the increase in heat transfer from the ocean to the atmosphere. Model estimates indicate that an increase of 4% in the area covered by leads during winter could produce a hemisphere-wide warming of 1 degree Kelvin [*Ledley*, 1988]. Understanding lead formation processes as well as the geographical and temporal distribution of lead networks is therefore important to studies of global climate.

Measurements of ice thickness and lead coverage are commonly made along transects using upward-looking submarine sonar. The footprint of the sonar beam used by submarines to observe ice conditions is of sufficiently high resolution, often 3 m or less as opposed to 25 m or more for satellite sensors, to make it a potentially useful instrument for gathering lead statistics. In fact, sonar data have shown that the largest number of lead widths are in the 10-20 m range. Lead width statistics derived from submarine sonar data have been reported in the literature [e.g., *McLaren*, 1989; *Wadhams*, 1981; *Wadhams and Horne*, 1980], but when lead orientation and width statistics are not available, the error in these analyses cannot be accessed. This error may be relatively small if leads are narrow or randomly oriented, but may be large in the case of wide leads or leads with a preferred orientation. While it may not be possible to determine the actual error for much of the archived sonar data, an important question concerns whether or not the data can be used for lead geometry statistics, and if so, what is the magnitude of the maximum error. In this paper a probabilistic determination of this error is described, providing a starting point for the application of stochastic geometry theorems in the analysis of lead geometries. Errors in statistics derived for other lead and keel features are discussed briefly. While the application is to sea ice leads and sonar data, the methods also apply to the general problem of sampling linear features along a transect.

Paper number 91JC01843.
0148-0227/91/JC-01843$05.00

2. DEFINITIONS, NOTATION, AND AN ILLUSTRATION

In the following discussions, notation follows that used in probability theory, where $F_Z(z)$ denotes the distribution function (df) for the population random variable Z with specific instance z (i.e., $F_Z(z) \equiv P[Z < z]$) and $f_Z(z)$ is the probability density function (pdf). Additionally, $E[Z]$ and $\mathrm{Var}[Z]$ are the expected value and variance of Z.

The problem is to relate a distribution of lead widths taken along a line perpendicular to the local orientation of a lead (the "actual" width) to the lead widths measured along a transect (the "apparent" lead width), taking into account lead orientations, and lead crossing angles. As illustrated in Figure 1, the following continuous random variables are defined: X is actual lead width, X' is apparent lead width measured along a transect, Θ is lead orientation ($0 \le \Theta < \pi$), and A is lead intersection angle ($0 \le A < \pi$), with specific realizations x, x', θ, and α. Additionally, let ϕ be the transect orientation ($0 \le \phi < \pi$). The position and orientation of a lead within the plane are uniquely specified by the length of the perpendicular that connects the lead to the origin, and the angle that it makes with a fixed reference line. The intersection angle A is measured between the transect and the lead, anticlockwise, and is the difference between their orientations.

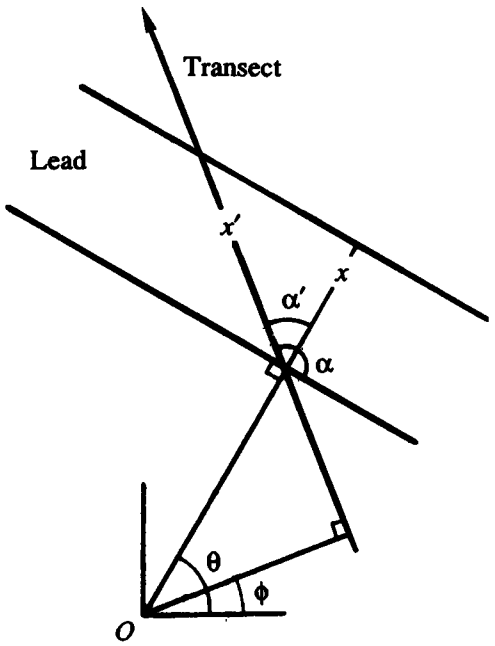

Fig. 1. The geometrical relationships between a lead and a transect. See text for definition of angles and length variables.

Finally, define $A' = |\pi/2 - A|$ to be the crossing angle (α' in Figure 1) measured between the transect and a perpendicular to the lead orientation ($0 \le A' \le \pi/2$). The relationship between apparent and actual lead widths is

$$X' = \frac{X}{\cos(A')} \quad (1)$$

where $X \le X'$. Rearranging terms, a lead crossing angle can be determined from the lead widths by

$$A' = \cos^{-1}\left(\frac{X}{X'}\right)$$

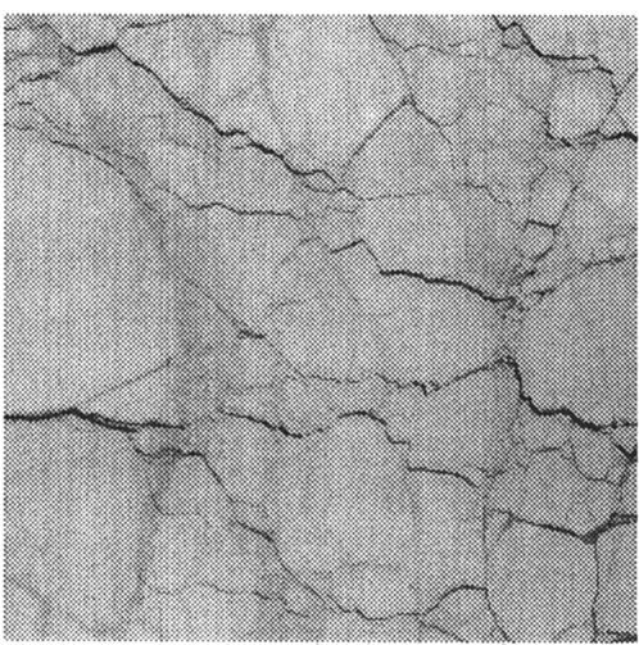

Fig. 2. Landsat MSS band 4 scene of the ice pack north of Alaska in March 1988. Area covered is approximately $(80 \text{ km})^2$. Field-of-view is 80 m.

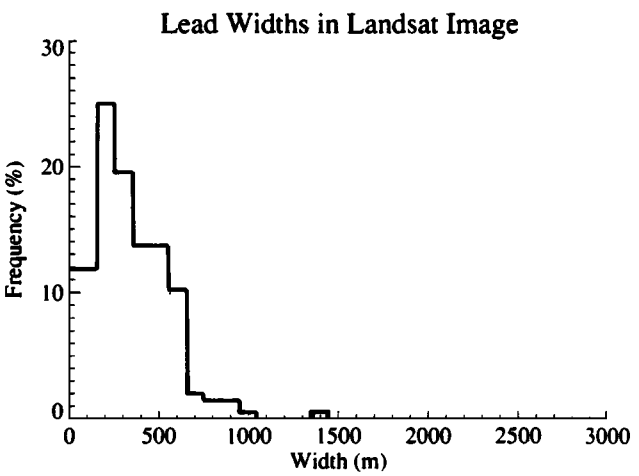

Fig. 3. Lead width distribution for the scene in Figure 2. Widths are measured along a perpendicular to the local orientation of the lead, and are grouped in 100 m bins. The mean width is 348 m, the standard deviation 201 m, and maximum width 1376 m.

The potential inaccuracies of measuring lead widths along a transect can be illustrated by randomly choosing a transect orientation and location on a satellite image. Here we provide an example with a Landsat Multispectral Scanner (MSS) band 4 (0.5-0.6 μm) scene of the Beaufort Sea, March 1988 (Figure 2). The pixel size is 80 m; image size is 80 x 80 km, a subset of a Landsat scene. To increase the sample size of lead widths measured along the transect, multiple transects of the same orientation are placed randomly on the image. It is assumed that the pattern of leads is similar beyond the image boundaries. Processing of the Landsat data for the retrieval of lead statistics is as follows. A dynamic threshold procedure is applied that estimates the probability density function of a mixture population (lead/ice) for small regions within the image, and a binary image results. Valid lead fragments are identified, where "valid" refers to a linear feature for which a meaningful width and orientation can be determined. Linearity is determined through correlation/regression analysis. Lead widths are measured perpendicular to the regression line, every kilometer along the lead length, and the slope of the regression line is a measure of the

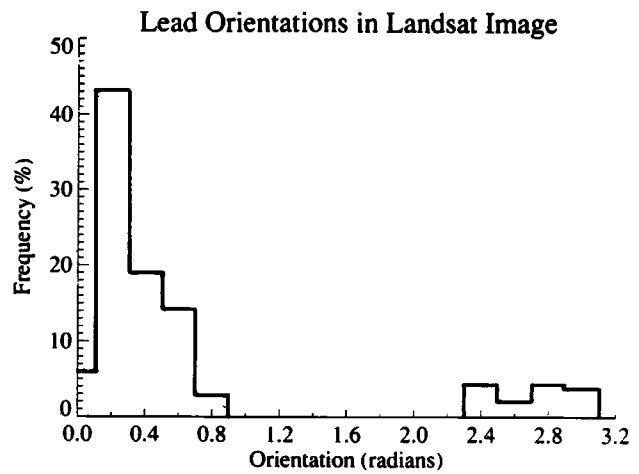

Fig. 4. Lead orientations for the scene in Figure 2. The mean orientation is 0.67^r (38.4°) with standard deviation 0.87^r (49.8°).

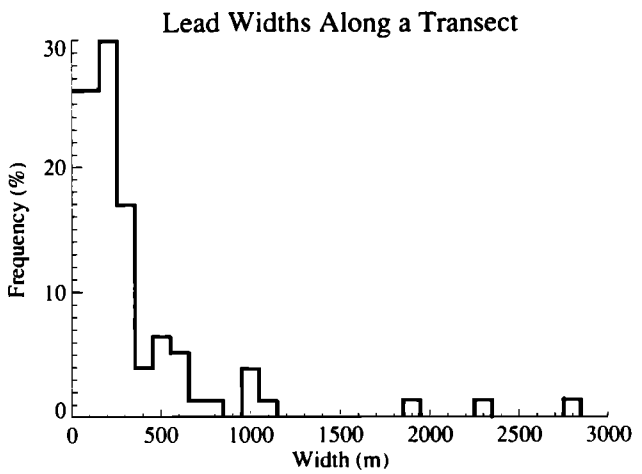

Fig. 5. Lead widths from a randomly chosen transect across Figure 2. Transect orientation is 3.0^r (172°) or approximately south-southwest to north-northeast where the top of the image is north. The mean width is 368 m, the standard deviation 474 m, and maximum width 2818 m.

lead orientation. Further details of this procedure are given in *Key et al.* [1990].

The distribution of these actual lead widths x is shown in Figure 3 and orientations θ in Figure 4. The mean lead orientation is 0.67 radians (38°, approximately southeast to northwest where the top of the image is north). For a transect orientation ϕ=3.0 radians (172°, south-southwest to north-northeast), the distribution of apparent lead widths x' is illustrated in Figure 5, with crossing angles α' shown in Figure 6. The mean actual width is 348 m with a standard deviation of 201 m, while the mean apparent width is 368 m with a standard deviation of 474 m. Additionally, the maximum actual lead width in the image is 1376 m, while the maximum width measured along the transect is 2818 m. With a transect orientation of 0.13 radians (7.4°) the difference between the actual and apparent mean widths is 139 m and the maximum width is 2670 m. From this example it is clear that significant errors can result from sampling along a transect. The following section presents a method to assess this error.

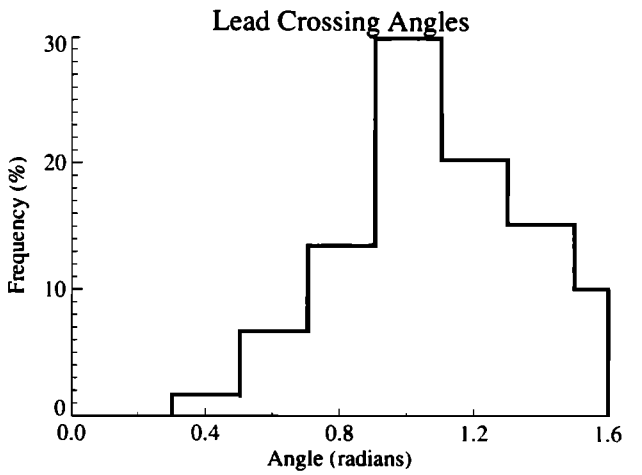

Fig. 6. Lead crossing angles for a transect across Figure 2. Transect orientation is the same as in Figure 5. The mean crossing angle is 1.09^r (62°) with standard deviation 0.23^r (13°).

3. Probability Models

Theorems of stochastic geometry that are applicable here have been developed through the study of fibers as a stationary random process in the plane. If we use this analogy with lead networks, then after *Stoyan et al.* [1987, p. 240] the df of intersection angles is

$$F_A(\alpha) = \frac{\int_{\phi}^{\phi+\alpha} \sin(\theta' - \phi)\, dF_\Theta(\theta')}{\int_0^{\pi} |\sin(\theta' - \phi)|\, dF_\Theta(\theta')} \qquad (2)$$

where $F_A(\alpha)$ is the probability of intersection angles between 0 and α, $F_\Theta(\theta)$ is distribution function for lead orientations, $dF_\Theta(\theta) = f_\Theta(\theta)\, d\theta$, α increases in an anticlockwise sense, and in the integral $F_\Theta(\pi + \alpha) = 1 + F_\Theta(\alpha)$. The pdf $f_\Theta(\theta)$ may be an assumed mathematical distribution or may be based on an observed rose of direction.

If the leads are isotropic then the corresponding orientations have a simple uniform probability distribution in the interval $0 \le \theta < \pi$; i.e., $f_\Theta(\theta)=1/\pi$ for all θ. In this case the distribution of intersection angles is independent of the transect orientation. The probability of crossing a lead that is oriented across the transect ($\alpha \to \pi/2$) is greater than for one running more parallel ($\alpha \to 0$ or π). The associated intersection angles have density

$$f_A(\alpha) = \tfrac{1}{2} \sin\alpha \quad , 0 \le \alpha \le \pi$$

which is not uniform but is symmetrical about $\alpha = \pi/2$. The corresponding distribution function is

$$F_A(\alpha) = \int_0^{\alpha} f_A(\psi)\, d\psi = \tfrac{1}{2}(1 - \cos\alpha) \quad , 0 \le \alpha \le \pi$$

which is a special case of (2) for $f_\Theta(\theta) = 1/\pi$. In the anisotropic (preferred orientation) case we use (2) for the distribution of intersection angles, and the corresponding densities are determined numerically.

Two different intersection angles correspond to each crossing angle so that the distribution and density functions for the crossing angle are

$$\begin{aligned} F_{A'}(\alpha') &\equiv P[A' \le \alpha'] \\ &= P[|\tfrac{\pi}{2} - A| \le \alpha'] \\ &= P[-\alpha' \le (A - \tfrac{\pi}{2}) \le \alpha'] \\ &= P[(\tfrac{\pi}{2} - \alpha') \le A \le (\tfrac{\pi}{2} + \alpha')] \\ &= F_A(\tfrac{\pi}{2} + \alpha') - F_A(\tfrac{\pi}{2} - \alpha') \end{aligned}$$

and

$$f_{A'}(\alpha') = \frac{dF_{A'}}{d\alpha'} = f_A(\tfrac{\pi}{2} + \alpha') + f_A(\tfrac{\pi}{2} - \alpha')$$

which in the isotropic case yields $F_{A'}(\alpha') = \sin\alpha'$ and $f_{A'}(\alpha') = \cos\alpha'$.

3.1. *Width Distributions*

An expression for the joint density function of the apparent and actual lead widths can be derived. Suppose that the joint pdf of X and A' are known, which will be $f_{X,A'}(x,\alpha') = f_X(x) f_{A'}(\alpha')$ if the two variables are independent. Then if Y and Z are two new random variables that are functions of X and A' such that $Y = X$ and $Z = X' = X/\cos A'$, then the joint pdf of Y and Z can be computed using a standard theorem [*Ross*, 1984, p. 217]:

$$f_{Y,Z}(y,z) \equiv f_{X,X'}(x,x')$$
$$= f_{X,A'}[x,\cos^{-1}(\frac{x}{x'})] \frac{x}{x'} [(x')^2 - x^2]^{-1/2}$$
$$= f_X(x)\, f_{A'}[\cos^{-1}(\frac{x}{x'})] \frac{x}{x'} [(x')^2 - x^2]^{-1/2} \quad (3)$$

The first of these expressions is valid whether or not X and A' are independent. If, however, future research indicates that large leads are oriented differently than small leads, for example, then the joint density function must be determined in another manner (possibly from observations). Using (3), the pdf of apparent lead widths can be obtained:

$$f_{X'}(x') = \int_0^\infty f_{X,X'}(x,x')\, dx$$
$$= \int_0^{x'} f_X(x) \{f_{A'}[\cos^{-1}(\frac{x}{x'})] \frac{x}{x'} \times [(x')^2 - x^2]^{-1/2}\}\, dx \quad (4)$$

The df of apparent lead widths can be obtained by integrating (4) or by conditioning on the value of X, again assuming that X and A' are independent. The latter method yields

$$F_{X'}(x') = \int_0^{x'} F_{A'}[\cos^{-1}(\frac{x}{x'})] f_X(x)\, dx \quad (5)$$

which is based on the df rather than the pdf of A'.

Determining the distribution of actual lead widths given the apparent lead width distribution must be approached differently. Letting $Y = 1/\cos A'$, then (1) can be rewritten as

$$X' = XY$$
$$\log X' = \log X + \log Y$$

X and A' are assumed to be independent, hence so are $\log X$ and $\log A'$, so that $\log X'$ is a sum of two independent random variables. This allows us to write

$$f_{\log X'} = f_{\log X} * f_{\log Y} \quad (6)$$

or

$$F_{\log X'} = F_{\log X} * f_{\log Y} \quad (7)$$

where the asterisk represents convolution [*Ross*, 1984, p. 202]. The Laplace transform may be used with either (6) or (7). The Fourier transform may be used with (6) but not with (7) because the pdfs are absolutely integrable but the df is not. Using $\varphi[f]$ to denote the Fourier transform of f, then with (6)

$$\varphi[f_{\log X'}] = \varphi[f_{\log X} * f_{\log Y}] = \varphi[f_{\log X}]\varphi[f_{\log Y}]$$
$$f_{\log X} = \varphi^{-1}\left\{\frac{\varphi[f_{\log X'}]}{\varphi[f_{\log Y}]}\right\}$$

from which the actual lead width distribution is

$$f_X(x) = \frac{1}{x}\, \varphi^{-1}\left\{\frac{\varphi[f_{\log X'}]}{\varphi[f_{\log Y}]}\right\}(\log x) \quad (8)$$

The derivation of (8) is given in the appendix. This expression shows that when the appropriate transforms exist, then the pdf of X is uniquely determined in terms of the pdfs of X' and A'. However, it is only useful for computations if the Fourier transforms and inverse transforms shown can be performed analytically. This is because in practice the inverse transform is an array of numbers that must be evaluated at $\log x$, which becomes a sampling problem with discrete data; i.e., a very large number of observations sampled at small intervals would be necessary for any reasonable degree of success with this approach.

Fortunately, there is another way to approach the problem. Referring back to (4) and (5), $f_{X'}$ and $F_{X'}$ can be viewed as the result of applying an integral operator to f_X. The functions can be discretized as arrays and the integral in (5) approximated as a sum:

$$F_{X'}(j) = \Delta \sum_{i=1}^{j} F_{A'}(j,i)\, f_X(i), \quad i, j \in [1,N],\ x = i\Delta,\ y = j\Delta \quad (9)$$

where $F_{A'}(j,i) = F_{A'}[\cos^{-1}(i/j)]$, N is the number of discrete observations and Δ is the increment between observations. If these functions are expressed as matrices, (9) becomes

$$\boldsymbol{F_{X'}} = \Delta\, \boldsymbol{F_{A'}}\, \boldsymbol{f_X}$$
$$\boldsymbol{f_X} = \frac{1}{\Delta}\, \boldsymbol{F_{A'}^{-1}}\, \boldsymbol{F_{X'}}$$

whose derivation is given in the appendix.

3.2. *Error Distribution*

In this study the error in measured lead width is defined as X'-X (which is always positive), although other definitions such as X/X' would also be useful. Equation (3) allows us to compute the distribution of the error as follows:

$$F_{X'-X}(a) \equiv P[X'-X \le a]$$
$$= \int_0^\infty \int_x^{a+x} f_{X,X'}(x,x')\, dx'\, dx, \quad a \ge 0$$

For the isotropic case

$$F_{X'-X}(a) = \int_0^\infty f_X(x) \sqrt{a} \left[\frac{\sqrt{2x + a}}{x + a}\right] dx$$

All moments of X'-X can be computed from $f_{X'-X}$.

4. APPLICATION

These models are now applied. First, a lead width distribution measured from sonar data is used to estimate the actual lead width distribution, for both isotropic and anisotropic orientations. Lead orientation and actual width distributions are then assumed known, and expected error in lead width is determined for a variety of situations.

Lead width distributions have been described by power laws [*Wadhams*, 1981; *Steffen*, 1987] as have floe sizes [*Rothrock and Thorndike*, 1984]. The negative exponential distribution has also been used [*Dickins et al.*, 1986]:

$$f_X(x) = e^{-x/\lambda} / \lambda$$

with mean lead width λ and variance λ^2. The exponential model implies that there are a finite number of small leads, and that the field is characterized by a length scale λ. In fact, the lead width distribution may be scale-free, in which case a power law would be appropriate. There is, of course, a lower limit imposed by the resolution of the measuring instrument, and for this reason as well as for clarity of illustrating expected values, we use the negative exponential model.

Lead orientations may be random or may have a preferred orientation. A Gaussian model is used here for

TABLE 1. Expected Error in Lead Widths (in Meters) Under a Variety of Assumed Distributions and Mean Values

Case	f_X*	$f_{X'}$	f_Θ	ϕ^r	$E(X - X')$	$\mathrm{Var}(X - X')$
1	?	Sonar	Uniform	---	65.7	1466.1
2	λ=20m	?	Gaussian†	2.36 (135°)	3.7	3.1
3	λ=20m	?	Gaussian†	0.52 (30°)	32.5	165.9
4	λ=40m	?	Gaussian†	2.36 (135°)	4.8	6.4
5	λ=40m	?	Gaussian†	0.52 (30°)	36.0	345.3
6	λ=20m	?	Uniform	---	43.2	653.1
7	λ=40m	?	Uniform	---	64.2	1391.2

Question marks refer to the unknown distribution.
* Width distribution model is negative exponential.
† Parameters of the Gaussian model are $\mu=\pi/4^r$ (45°) and $\sigma=0.3^r$ (17°).

preferred orientations. It is recognized, however, that the actual shape of the distribution may be bimodal, where large leads with one orientation are intersected by smaller leads at another. Intersection angles of approximately 28° have been observed elsewhere [*Marko and Thomson*, 1977]. This situation is not obvious in Figure 4, although the distribution is not strictly Gaussian either.

Table 1 lists the expected error for a variety of conditions, where error is defined by the difference between the actual and measured lead widths. Case 1 considers the situation where the apparent lead width distribution is known. The apparent lead widths are based on submarine sonar data recorded by the USS QUEENFISH in August of 1970 in the central Canada Basin [*McLaren*, 1989]. Ice draft data were measured by an upward-beamed fathometer with a footprint diameter of approximately 2.7 m and a vertical accuracy of ±10 cm. Sequences of continuous points with drafts ≤30 cm constitute leads, an example of which is given in Figure 7. The apparent width distribution was determined for a 100 km section and is shown in Table 2. Given a mean apparent lead width of 60.6 m, the expected value of the error is 65.7 m with a variance of 1466.1 m^2. For cases 2-7 in Table 1 the actual width density function is assumed known, and the apparent lead width distribution is estimated. For cases 2 and 3, the crossing angle distributions are shown in Figure 8, and the error distributions in Figure 9. In the preferred orientation cases (2-5) the error means and variances are clearly dependent upon transect orientation.

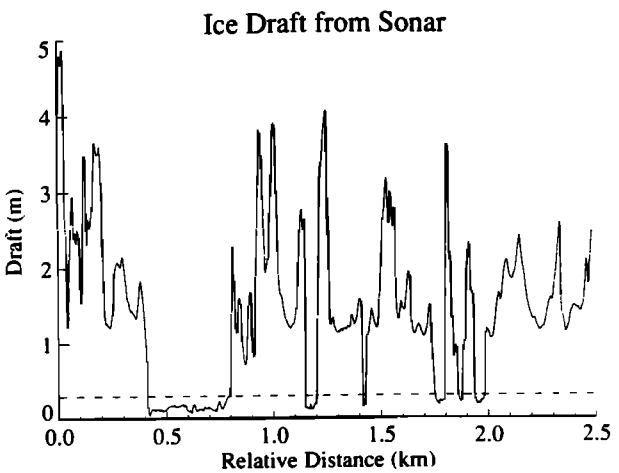

Fig. 7. Submarine sonar ice draft data for a 2.5 km section within the Canada Basin north of Alaska. Leads are defined as continuous sequences of points with drafts no greater than 0.3 m (dashed line); six leads occur in this section.

5. CONCLUSIONS

A methodology has been presented for determining width distributions of linear features from measurements along a transect through a network of such features. Both isotropic and anisotropic orientations of the linear features have been considered. In the anisotropic case, the orientation distribution of the lines must be known. In both cases if the distribution of actual widths and the orientations are viewed as independent random variables then the actual width distribution can be determined from the

TABLE 2. Lead Widths (Bin Midpoint) and Number of Leads per Bin, Measured by Submarine Sonar

Width	N	Relative Frequency
20.00	134	0.441
40.00	63	0.207
60.00	18	0.059
80.00	25	0.082
100.00	22	0.072
120.00	12	0.039
140.00	4	0.013
160.00	4	0.013
180.00	5	0.016
200.00	5	0.016
220.00	3	0.010
240.00	2	0.007
260.00	0	0.000
280.00	0	0.000
300.00	3	0.010
320.00	0	0.000
340.00	1	0.003
360.00	3	0.010

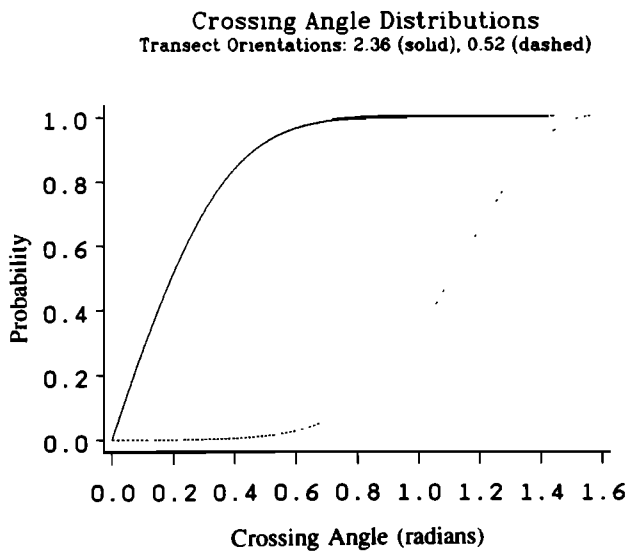

Fig. 8. The distribution functions of crossing angles F_A, for cases 2 (solid) and 3 (dashed) in Table 1.

apparent widths and vice versa. Furthermore, if the actual widths and the orientations vary jointly then the apparent width can be determined from the joint distribution. The application presented was to measurements of sea ice leads made by submarine sonar. The width distributions measured from sonar illustrated that the general shape is similar to those derived from satellite imagery, but that the errors in widths can be significant. Unfortunately, it is not possible to determine the actual error in lead widths derived from much of the archived sonar data. However, if lead "climatologies" can be compiled for various locations and seasons, or if significant relationships between lead orientation and geostrophic winds can be developed, then at least we can determine the probable error.

Of course, the potential error is not an issue if adequate two-dimensional data are available. For example, side-scan sonar may permit a more accurate retrieval of lead and keel statistics [*Wadhams*, 1988]. Sonar data with concurrent overhead imagery from aircraft or satellite is also a potentially valuable source of information. However, lead width distributions derived from satellite data may not be accurate since very small leads are not resolved. This is particularly true for medium resolution data such as that from the Defense Meteorological Satellite Program (DMSP) or the Advanced Very High Resolution Radiometer (AVHRR) on-board the TIROS-N satellites. One solution might be to retrieve the orientation information from satellite data where small lead widths cannot be resolved, and the width information from submarine sonar transects.

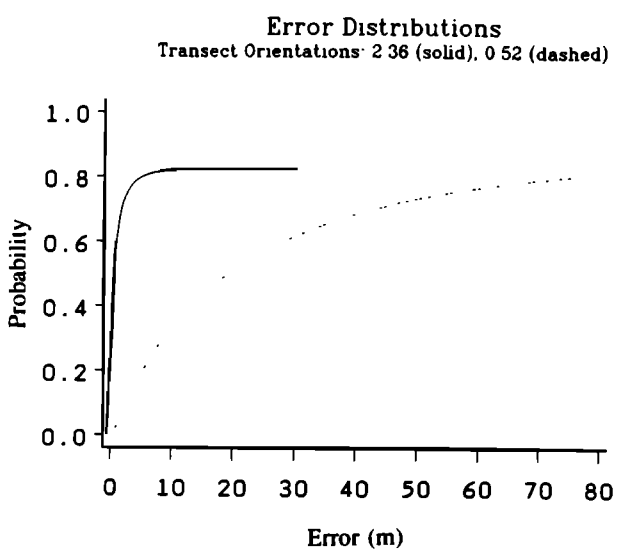

Fig. 9. The distribution functions of the lead width errors, $F_{X'-X}$, for cases 2 (solid) and 3 (dashed) in Table 1.

Other applications of this procedure are possible. For example, laser profilometer transects are analogous to sonar transects, and the methods outlined above could be used for lead and ridge spacing distributions and their associated errors. As in the illustration with Landsat data, transect sampling of satellite imagery is a natural application. Similarly, heat flux through leads is in part a function of fetch, and fetch is a function of the actual lead width and the crossing angle of the wind. If the wind direction is constant as it travels across the network of leads, then the distribution of fetches can be determined from the distribution of actual lead widths. Finally, it may be possible to estimate open water fraction over a large area from the apparent lead width and spacing distributions measured along a transect. This research is currently in progress, with results to be presented subsequently.

APPENDIX

Derivation of f_X From $f_{\log X}$

Equation (6) gives an expression for $f_{\log X}$. However, we are interested in f_X rather than $f_{\log X}$, so we use the identity

$$f_{\log Y}(\log y) = y\, f_Y(y) \tag{A1}$$

which is proven by

$$\begin{aligned} F_{\log Y}(\log y) &= P[\log Y \le \log y] \\ &= P[e^{\log Y} \le e^{\log y}] \\ &= P[Y \le y] \\ &= F_Y(y) \end{aligned}$$

The derivative of both sides with respect to y produces (A1).

Using (A1) and (6), an expression for the actual lead width distribution can be obtained:

$$f_{\log X}(\log x) = \varphi^{-1}\left\{\frac{\varphi[f_{\log X'}]}{\varphi[f_{\log Y}]}\right\}(\log x)$$

$$f_X(x) = \frac{1}{x}\,\varphi^{-1}\left\{\frac{\varphi[f_{\log X'}]}{\varphi[f_{\log Y}]}\right\}(\log x) \tag{A2}$$

Matrix Formulation of f_X

Expressing equation (5) in terms of matrices provides a way to solve for f_X. The functions can be discretized as arrays and the integral approximated as a sum as shown in (9), which is repeated here:

$$F_{X'}(j) = \Delta \sum_{i=1}^{j} F_{A'}(j,i) f_X(i), \tag{9'}$$

$$i,j \in [1,N],\ x = i\Delta,\ y = j\Delta$$

where $F_{A'}(j,i) = F_{A'}[\cos^{-1}(i/j)]$, N is the number of discrete observations and Δ is the increment between observations. Suppose we now form an N x N matrix, M, as follows:

$$M(j,i) = \Delta F_{A'}(j,i), \quad 1 \le i \le j \le N$$
$$M(j,i) = 0, \quad 1 \le j < i \le N$$

where the first expression refers to elements on or below the diagonal. It follows that

$$\Delta \sum_{i=1}^{j} F_{A'}(j,i) f_X(i) = \sum_{i=1}^{N} M(j,i) f_X(i) \qquad \text{(A3)}$$

or

$$F_{X'}(j) = \sum_{i=1}^{N} M(j,i) f_X(i) \qquad \text{(A4)}$$

This is equivalent to the matrix equation

$$F_{X'} = M f_x \qquad \text{(A5)}$$

From this it can be seen that the problem is solved if M is invertible. However, since $M(j,j) = F_{A'}(j,j) = 0$ for all j (from the definition of $F_{A'}$), the matrix M has zeros on as well as above the diagonal, therefore the first row and last column contain all zeros, so that $\det(M) = 0$, or M is not invertible.

This difficulty is overcome by defining a new N-1 x N-1 matrix M_2 to be the submatrix formed by deleting the first row and last column from M. This gives

$$\begin{pmatrix} f_1 \\ f_2 \\ \cdots \\ f_{N-1} \end{pmatrix} = M_2^{-1} \begin{pmatrix} F_2 \\ F_3 \\ \cdots \\ F_N \end{pmatrix} \qquad \text{(A6)}$$

where $f_X = (f_1, f_2, \ldots, f_N)$ and $F_{X'} = (F_1, F_2, \ldots, F_N)$. Since $F_1 = 0$, it is not needed to find $f_1, \ldots, f_N$. Furthermore, if N and Δ are chosen properly, then $f_N = 0$ because f is a pdf.

Acknowledgments. J. Key was supported by Office of Naval Research (ONR) grant N00014-90-J-1840. S. Peckham was supported under a NASA Global Change Research Student Fellowship. Thanks are due to A.S. McLaren for providing the submarine sonar data (ONR University Research Initiative Program contract N00014-86-K-0695). We thank D. Rothrock for comments on an earlier version of this paper.

REFERENCES

Dickins, D., A. Dickinson, and B. Humphrey, Pack ice in Canadian waters: dimensions and dynamics of leads and floes, unpublished report to the Environmental Emergencies Technology Division, Environmental Protection Service, Ottawa, Ontario, 62 pp., April 1986.

Key, J., A.J. Schweiger, and J.A. Maslanik, Mapping sea ice leads with a coupled numeric/symbolic system, in *Image Processing/Remote Sensing. ACSM/ASPRS Proceedings*, vol. 4, pp. 228-237, American Congress on Surveying and Mapping and American Society for Photogrammetry and Remote Sensing, Bethesda, MD, 1990.

Ledley, T., A coupled energy balance climate-sea ice model: impact of sea ice and leads on climate, *J. Geophys. Res.*, *93*(D12), 15,919-15,932, 1988.

Marko, J.R., and R.E. Thomson, Rectilinear leads and internal motions in the ice pack of the western Arctic Ocean, *J. Geophys. Res.*, *82*(6), 979-987, 1977.

McLaren, A.S., The under-ice thickness distribution of the Arctic Basin as recorded in 1958 and 1970, *J. Geophys. Res.*, *94*(C4), 4971-4983, 1989.

Ross, S., *A First Course in Probability*, 2nd ed., 392, Macmillan, New York, 1984.

Rothrock, D.A., and A.S. Thorndike, Measuring the sea ice floe size distribution, *J. Geophys. Res.*, *89*(C4), 6477-6486, 1984.

Steffen, K., Fractures in arctic winter pack ice (North Water, northern Baffin Bay), *Ann. Glaciol.*, *9*, 1-4, 1987.

Stoyan, D., W.S. Kendall, and J. Mecke, *Stochastic Geometry and Its Applications*, 345, John Wiley, New York, 1987.

Wadhams, P., Sea-ice topography of the Arctic Ocean in the region 70°W to 25°E, *Philos. Trans. R. Soc. London*, *302*, 45-85, 1981.

Wadhams, P., The underside of the Arctic sea ice imaged by sidescan sonar, *Nature*, *333*, 161-164, 1988.

Wadhams, P., and R.J. Horne, An analysis of ice profiles obtained by submarine sonar in the Beaufort Sea, *J. Glaciol.*, *25*(93), 401-424, 1980.

J. Key, Cooperative Institute for Research in Environmental Sciences, University of Colorado, Boulder, CO 80309-0449.

S. Peckham, Cooperative Institute for Research in Environmental Sciences, and Department of Geology, University of Colorado, Boulder, CO 80309-0449.

(Received November 8, 1990;
revised June 25, 1991;
accepted July 2, 1991.)